Acta Oceanol. Sin., 2014, Vol. 33, No. 7, P. 107–115
DOI: 10.1007/s13131-014-0510-x
http://www.hyxb.org.cn
E-mail: hyxbe@263.net

Wave-current bottom shear stresses and sediment re-suspension in the mouth bar of the Modaomen Estuary during the dry season

JIA Liangwen[1], REN Jie[1]*, NIE Dan[1], CHEN Benzhong[1], LV Xiaoying[1]

[1] Center for Coastal Ocean Science and Technology Research, Sun Yat-sen University, Guangzhou 510275, China

Received 21 July 2013; accepted 24 January 2014

Abstract

On the basis of the measurement data pertaining to waves, current, and sediment in February 2012 in the mouth bar of the Modaomen Estuary, the Soulsby formulae with an iterative method are applied to calculating bottom shear stresses (BSS) and their effect on a sediment re-suspension. Swell- induced BSS have been found to be the most important part of the BSS. In this study, the correlation coefficient between a wave-current shear stress and SSC is 0.86, and that between current shear stresses and SSC is only 0.40. The peaks of the SSC are consistent with the height and the BSS of the swell. The swell is the main mechanism for the sediment re-suspension, and the tidal current effect on sediment re-suspension is small. The peaks of the SSC are centered on the high tidal level, and the flood tide enhances the wave shear stresses and the SSC near the bottom. The critical shear stress for sediment re-suspension at the observation station is between 0.20 and 0.30 N/m^2. Tidal currents are too weak to stir up the bottom sediment into the flow, but a WCI (wave-current interaction) is strong enough to re-suspend the coarse sediment.

Key words: Modaomen Estuary, wave-current, bottom shear stresses, sediment

Citation: Jia Liangwen, Ren Jie, Nie Dan, Chen Benzhong, Lv Xiaoying. 2014. Wave-current bottom shear stresses and sediment re-suspension in the mouth bar of the Modaomen Estuary during the dry season. Acta Oceanologica Sinica, 33(7): 107–115, doi: 10.1007/s13131-014-0510-x

1 Introduction

In shallow coastal waters, both wave and current movements are significant and important to a sediment transport. Surface waves interacting with the seafloor can create turbulent boundary layers that make significant contributions to wave energy dynamics, dissipation rates, and fluid sediment interactions (Trowbridge and Madsen, 1984a, b; Mathisen and Madsen, 1996a,b; Styles and Glenn, 2002). It has been shown (Grant and Madsen, 1979) that when the wave and the current exist jointly in a region, shear stresses are altered because the turbulence generated by the wave-current interaction (WCI) near the bed is different from the stresses expected in the case of pure wave or pure current. There is a nonlinear interaction between the two flows, and the fluid dynamics are changed. So, the method to calculate the bed shear stress for combined wave and current conditions is somewhat more uncertain due to the possibility of the nonlinear interaction as the flow becomes more energetic (Soulsby et al., 1993; Soulsby, 1997). A number of models to describe the WCI within the bottom boundary layer have been proposed. They can be classified into time-invariant eddy-viscosity models and mixing-length models (Malarkey and Davies, 1998). The most representative of the time-invariant eddy-viscosity models are those proposed by Grant and Madsen (1979) and Christoffersen and Jonsson (1985). Based on the concept of Grant and Madsen (1979), the nonlinear wave-current combination shear stress formulae have been proposed by Soulsby et al. (1993) with an iterative method, now widely used in the calculation of the BSS under the WCI.

The BSS under the WCI have been investigated through the direct measurements (Jago et al., 1992; Hambling, 1989; Lavelle et al., 1984; Lou and Ridd, 1996; Rodolfo et al., 2012) as well as the modeling in various coastal environments in the world (Soulsby et al., 1993; Holmedal et al., 2003; Rosales et al., 2008; Shi and Wang, 2008). Lou and Ridd (1996) calculated the BSS using an iterative method based on the concept of Grant and Madsen (1979), employing the measurement data in Cleveland Bay, North Australia. Rosales et al. (2008) evaluated the effect of considering the WCI on the BSS calculations with a wave and current coupled model, and their study shows that when the WCI is taken into account, the calculated maximum bottom stress is usually doubled. The sediment transport under the WCI is closely related to the BSS, and some findings have also been uncovered in this area. On the basis of the critical condition for the initiation of sediment movement, according to a wide array of test data for a wave-current coexistent system, Cao et al. (2003) established the formulas of the sediment initial movement for both laminar and turbulent conditions. Kong et al. (2003) set up a theoretical formula of BSS for a wave-current coexisting system and obtained the condition of incipient movement of sand particles, the sediment carrying capacity, by means of the theory of boundary layers. In general, exceptional progress has been made in the wave-current BSS and the sediment transport research, but the field observations in various coastal environments and experiments are still insufficient. Owing to their

Foundation items: The Program of International S&T Cooperation under contract No. 2010DFA24470; the National Science Foundation of China under contract No. 41376101; the Guangdong Provincial Science and Technology Planning Project under contract Nos 2012A030200002 and 2011B031100008

*Corresponding author, E-mail address: Renjie@mail.sysu.edu.cn

complicated nature, much more work is still needed in this area.

As a particular example, the Modaomen Estuary (ME), located at the landward margin of the South China Sea shelf (Fig. 1), has evolved under coactions of various forcings such as the runoff, tide, wave, storm, and littoral current; this is a typical runoff and wave-dominant estuary in China. The sediment re-suspension under combined wave-current conditions is an important mechanism for the sediment transport and morphological evolution of the ME.

The role of the wave on the morphological evolution of the ME has been realized (Luo et al., 1983; Li, 1983; Li et al., 1993; Jia et al., 2009), but no research findings on the WCI are available. Owing to its potential economical importance, especially the navigation demand, much attention has been paid to the ME; the research on the WCI is also very necessary. In this paper, based on the measurement data in February 2012, The BSS were calculated, and their effects on the sediment re-suspension were analyzed using the Soulsby formulae with an iterative method. This study provides a quantitative understanding of the role of the WCI in the ME and may provide a good case for similar estuaries throughout the world.

2 Study area

The Modaomen Estuary (ME), located on the west wing of the Zhujiang River Delta (ZRD) (Fig. 1), is the main outlet of the Xijiang River. The runoff is strong, and the tide is relatively weak. The ratio of the multi annual mean runoff to the tidal prism is 5.77. The multi annual (1959–2010) mean runoff at the Makou Gauging Station (Fig. 1), where the Xijiang River enters the ZRD, is 7400 m^3/s. The monthly mean discharge varies from 11400 m^3/s during the wet season (April to September) to 3420 m^3/s during the dry season (October to March). The water discharge flowing into the ME accounts for 37.86% of that measured at the Sta. Makou. The tides at the ME are of irregular semi diurnal/mixed type. The annual mean tidal ranges at the tidal gauge stations Sanzao and Denglongshan are 1.11 and 0.86 m respectively. On the basis of the Dawanshan wave station at the south of the ME, the dominant wave direction is southeasterly with the occurrence of 71%. The monthly mean wave height ranges from 1.01 to 1.32 m with the average wave period from 5.15 to 5.70 s.

3 Data and methodology

The data for the calculation and analysis of the BSS in this paper were measured by the Center for Coastal Ocean Science and Technology Research, Sun Yat-sen University on February 18 to 23, 2012 (details below). The tidal elevation was collected from the Foshan Hydrology Bureau, Guangdong Province. The raw wave data were separated into a wind wave and swell wave based on the band separation frequency, 0.2 employed in this study. The nonlinear wave-current combination shear stress formulae proposed by Soulsby et al. (1993) with an iterative method are applied to calculating the BSS.

4 Field observation

The field observation was carried out from February 18 to 23, 2012. The measurements in all campaigns consist of installing five mooring stations in the estuary, among which the observation period at Stations M2 and M4 was from February 18

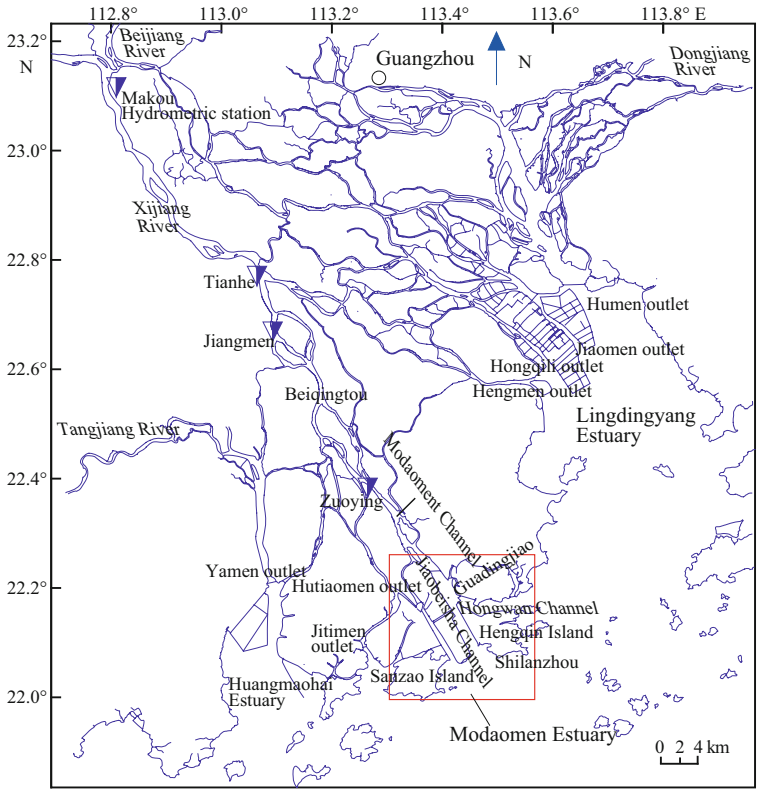

Fig.1. Location of the Modaomen Estuary.

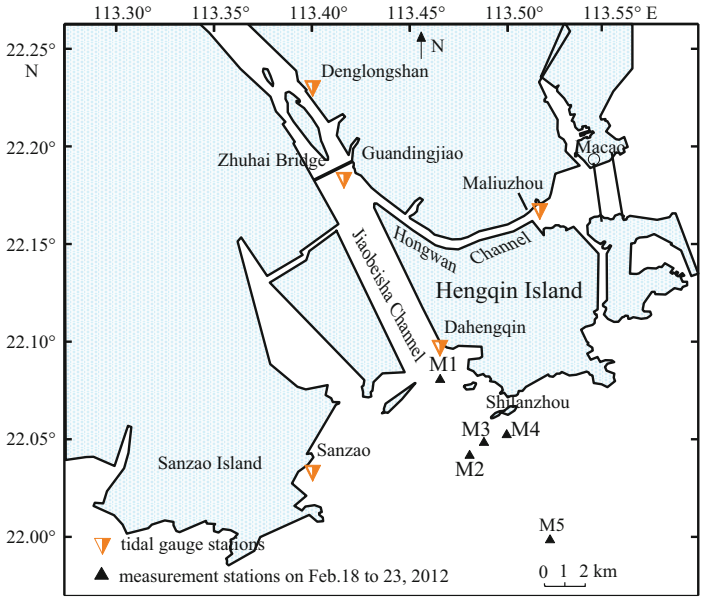

Fig.2. Locations of the measurement stations.

to 19. The stations were carefully designed to cover important morphological units. The locations of the stations are shown in Fig. 2. A Current, a salinity, a turbidity, and a wind were measured at each station. The ADPs (Acoustic Doppler Profiler) were mounted on fishery boats, and the downward-looking transducers were placed 0.5 m below the water surface. The ADPs were configured with 0.1 m bins and pinged at 2 Hz. They were programmed to sample 2 min bursts for every 5 min. OBSs (Optical Back Scatter) (Model 3A) were used for measuring water turbidity, temperature and salinity. The OBSs were lowered by winches from the water surface to the bottom within 1 min for obtaining the vertical profiles of the temperature, the salinity, and the turbidity every hour. In the meantime, water samples were collected and then taken to the laboratory for analysis. The water samples were filtered using 0.45 μm membrane filters. The membrane filters were then oven-dried, weighted, and calibrated. The thus-obtained SSC was contrasted to the turbidity data from the OBSs, and a conversion relationship was established for converting turbidity to SSC. The wave and bottom boundary layer were observed at Sta. M3, located in the inner slope of the mouth bar. The tripod with the two ADVs and one OBS-3A was installed, and one ADV was placed at 0.25 m above bottom and sampled at an interval of 900 s; another was placed at 1.35 m above bottom and sampled at an interval of 180 s to ensure the current data in the bottom boundary layer. The Nortek AWAC was placed at 0.6 m above bottom in the self-made steel support to measure the wave, and it was pinged at 2 Hz and sampled at an interval of 1 800 s. The parameters of the ADV, the OBS and the AWAC are shown in Table 1.

5 Wind, current and sediment during the measurement period

5.1 *Wind*

During the measurement period, a cold wave from the north hit the ZRD. At Sta. M3, the maximum wind speed measured was about 8 m/s, and the wind direction was mainly north or northeast (Fig. 3).

5.2 *Wave*

The significant height of the wind waves was between 0.2 and 0.6 m with a typical period of 2–3 s, while the significant

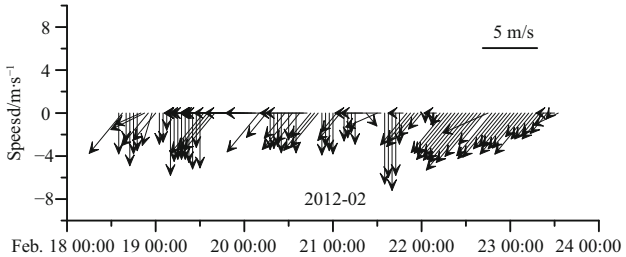

Fig.3. Wind vector during the measurement period.

Table 1. Parameters of the devices at the Sta. M3

Station	Period	Devices	sampling frequency/Hz	Distance from bottom/m	Measurement interval/s
M3	Feb. 18 11:00 to Feb. 23 11:00 (49 h)	ADV	32	0.25/1.35	180/900
		OBS	1	0.8	300
		AWAC	2	0.6	1 800

height of the swell was between 0.2 and 1.0 m with a typical period of 8–9 s. The wind wave and the swell came from the southeast with angles of 120°–160°. The swell wave height and the wind wave height were nearly the same, but their peaks differed (Fig. 4). There was a significant difference between the directions of wind and wave due to the wave refraction in the mouth bar.

5.3 *Current*

The direction of the ebb current was mainly southeast, and the velocity near the bottom could reach more than 0.60 m/s at Sta. M3 (Fig. 5). The direction of the flood current was mainly northeast, northwest, and north; and the maximum velocity near bottom was less than 0.34 m/s. The ebb tidal current duration was longer than the flood tidal current duration, and the

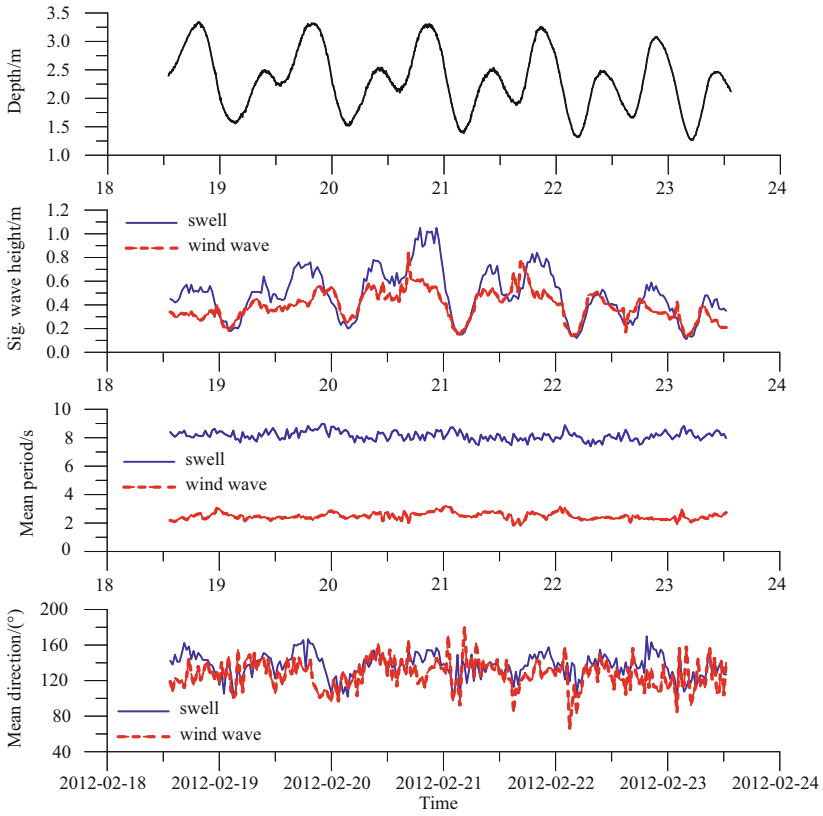

Fig.4. Height, period and direction of the waves.

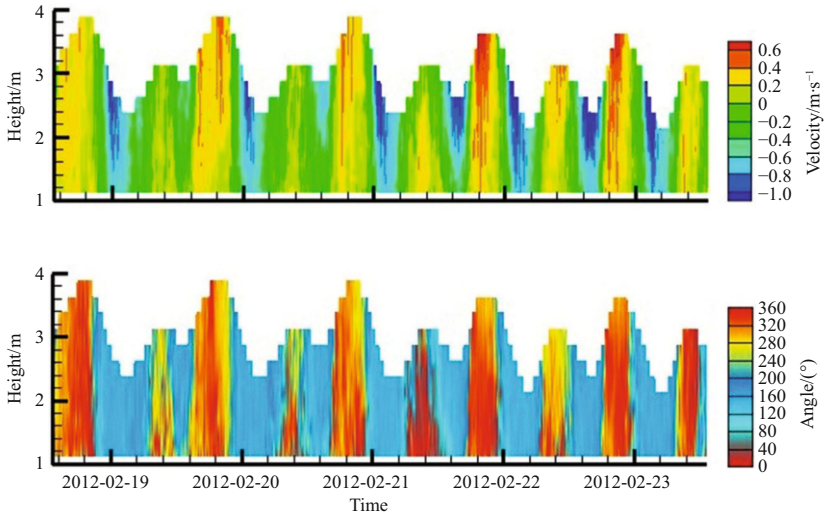

Fig.5. Velocity profile at the Sta. M3.

velocity of the ebb tidal current was larger than that of the flood tidal current, so the ebb tidal current was dominant.

5.4 *SSC*

The average SSC near the bottom at Sta. M3 was above 0.10 kg/m^3 with a maximum of 0.45 kg/m^3 (Fig. 6). The peaks of the SSC were consistent with those of the swell height. The maximum peak of the SSC occurred between 16:50–23:30 on February 20 with SSC being more than 0.23 kg/m^3 and the maximum being 0.44 kg/m^3 at 21:00, correspondent with the peak of the swell height.

6 Wave-current BSS

6.1 *Calculation method*

The effect of the WCI on the BSS is calculated based on the theory of Grant and Madsen (1979). In this theory, the current at the outer edge of boundary layer feels an enhanced drag that is a function of: (1) the near bottom wave orbital velocity U_w, (2) the mean current U_w, (3) the wave frequency ω, (4) the physical bottom roughness z_0, and (5) the angle between the wave propagation direction and the current φ_c. The reference level δ_{cw}, where the BSS are calculated is taken as the wave-current boundary layer thickness which is assumed to be 5% of the mean water depth. The mean water depth of the Sta. M3 is 4 m; δ_{cw} approximates to 0.2 m, consistent with the depth of the installed ADV.

The maximum bottom stress $\tau_{b,max}$ for the wave-current combination is given by

$$\tau_{b,max} = \tau_w + \tau_c , \tag{1}$$

where, the wave bed stress based on wave-induced u_{*w} (shear velocity/friction velocity) is given by

$$\tau_w = \rho u_{*w}^2 = \frac{1}{2}\rho f_w U_w^2 , \tag{2}$$

where ρ is the water density; τ_c is the current shear stress. $\tau_{b,max}$ is the maximum wave bed stress; $U_w = \frac{0.5H\omega}{\sinh(kh)}$ is the near bottom wave orbital velocity, which can be determined by the linear wave theory; and the wave friction factor f_w can be calculated as proposed by Jonsson (1966):

$$f_w = \exp\left[-6 + 5.2\left(\frac{A_\delta}{k_s}\right)^{-0.19}\right], \tag{3}$$

or calculated as proposed by Swart (1974):

$$f_w = 0.00251\exp\left[5.21\left(\frac{A_\delta}{k_s}\right)^{-0.19}\right],\ f_{w,max} = 0.3 \quad \text{for} \quad A_\delta / k_s \leqslant 1.57,$$

in which k_s is the bottom physical roughness, A_δ is the near bottom excursion amplitude, and $A_\delta = U_w T/2\pi$, T is the wave period.

An initial current friction factor f_c, not considering the wave effect, can be obtained by:

$$f_c = 2\left[\frac{\kappa}{\ln(30\delta_{cw}/k_s)}\right]^2 \tag{4}$$

where κ is von Karman's constant (0.4); and k_s is the bottom physical roughness (which is usually used to determine the bottom roughness height), and $z_0 = k_s/30$ in the turbulent condition. k_s is composed of three physical roughness measurements: (1) the particle roughness $k_{sg} = 2.5D$; (2) the bed form roughness $k_{sd} = 27.7H^2/\lambda$, where H and λ are the height and the length of the sand wave respectively; (3) the bed load roughness, $k_{sc} = 1.1424D\frac{\tau_{sf}}{\tau_c + 0.2\tau_{sf}}$ for $\tau_{sf} > \tau_{cr}$, in which τ_{cr} is the critical stress of sediment movement (shields parameter related to particle size of D).

The shear friction velocity can be obtained when considering the current only, as follows:

$$u_{*c} = \sqrt{\frac{1}{2}f_c}u_c , \tag{5}$$

by the shear stress $\tau_c = \rho u_{*c}{}^2 = \frac{1}{2}\rho f_c u_c{}^2$, where u_c is the current at the reference height δ_{cw}. $u_{*w} = \sqrt{\frac{1}{2}f_w}U_w$ can be obtained by Eq. (2). The combined wave-current friction velocities can be computed by

$$u_{*cw} = \left(u^2{}_{*c} + u^2{}_{*w} + 2u_{*w}u_{*c}\cos\varphi_c\right)^{1/2}. \tag{6}$$

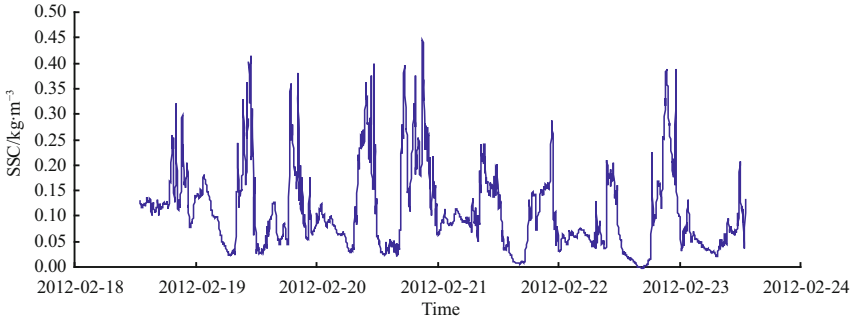

Fig.6. SSC near the bottom during the measurement period.

The apparent bottom roughness k_b (Signell et al., 1990), which indicates the turbulence level due to the combination of the wave-current boundary layer and the physical bottom roughness, can be calculated by

$$k_b = k_s \left[24 \frac{u_{*cw}}{U_w} \frac{A_\delta}{k_s} \right]^\beta , \quad (7)$$

where

$$\beta = 1 - \frac{u_{*c}}{u_{*cw}} . \quad (8)$$

The obtained value of k_b is then used in Eq. (4) to substitute the physical roughness k_s to determine a new estimate of the wave-current friction coefficient f_{cw} at the next time step by:

$$f_{cw} = 2 \left[\frac{\kappa}{\ln(30\delta_{cw} / k_b)} \right]^2 . \quad (9)$$

One may proceed by substituting f_{cw} for f_c in Eq. (5) and repeating the process from Eqs (5) to (9) until the successive estimates of f_{cw} differ by less than a preset error value (10^{-6} in this work). Having obtained the stable f_{cw}, the current shear stress, $\tau_c = \frac{1}{2} \rho f_{cw} u_c^2$, can be calculated in the presence of the wave.

Not considering the effect of the wave and current propagation directions on the wave-current combination shear stress, the maximum bottom stress $\tau_{b,max}$ for the wave-current combination is given by Eq. (1). The nonlinear wave-current combination shear stress proposed by Soulsby et al. (1993) can also be taken into consideration.

$$\tau_{cw} = \left[\left(\tau_m + \tau_w \left| \cos \varphi_c \right| \right)^2 + \left(\tau_w \sin \varphi_c \right)^2 \right]^{0.5} ,$$

$$\tau_m = \tau_c \left[1 + 1.2 \left(\frac{\tau_w}{\tau_w + \tau_c} \right)^{3.2} \right] .$$

where τ_m is the mean shear stress in the current direction; and τ_{cw} is the maximum shear stress within a wave period. Apparently, the effect of the wave and current propagation directions has been considered in the Soulsby et al. (1993) formulae.

6.2 *Analysis*

6.2.1 *Composition of shear stresses*

Both the wave height and the orbital velocity of the measured swell were much bigger than those of the wind waves. The maximum orbital velocity of the swell reached 0.75 m/s while that of the wind wave was less than 0.2 m/s (Fig. 7). The swell-, wind- and tidal-induced BSS are shown in Fig. 8. Obviously, the wave-current bottom stress is significantly greater than the bottom stress considering wave-induced τ_w only or tidal-induced τ_c only. The swell-induced bottom stress is between 1 and 2 N/m^2 with the maximum of 2.8 N/m^2, accounting for more than 73% of the total; the wind-induced bottom stress is generally less than 0.5 N/m^2, accounting for 16% of the total; the tidal-induced bottom stress fluctuates with the tide, reaching a maximum of 0.8 N/m^2 during the peak ebb and less than 0.2 N/m^2 during the flood tide, accounting for 11% of the total.

6.2.2 *Correlation between BSS and SSC*

In the ME, the highest SSC usually occurs in the mouth bar area. During the measurement period at Sta.M1, the landward mouth bar, the vertical mean SSC and the bottom SSC were 0.05 and 0.08 kg/m^3 respectively; at Sta.M5, at the seaward mouth bar, the vertical mean SSC and bottom SSC were 0.012 and 0.07 kg/m^3 respectively. However at Sta. M3, the mean bottom SSC was above 0.10 kg/m^3. Therefore, the water bodies from the ebb tidal current and flood tidal current could not remarkably increase the SSC at Sta. M3. It is also possible that the flocculation increased the SSC near the bottom in the estuarine salty environment. During the high peak of the wave height, the strong disturbance was not conducive to flocculation, but during the low wave height, when there was greater flocculation, the measured SSC near the bottom was always low, and so it is supposed that the flocculation had little effect on the SSC near the bottom. In addition, there were no human activities such as dredging and reclamation to suddenly increase the SSC during the measurement; therefore, the SSC at Sta. M3 was mainly induced by the sediment re-suspension under the action of the BSS.

The correlation coefficients between stresses induced by the tidal currents, the wind, the swell, the wave-current, and the SSC are listed in Table 2. It shows that the correlation between the wave-current shear stresses and the SSC is highest; the correlation between the swell-induced shear stresses and SSC is very high; the current stress is poorly correlated with the SSC. The bottom orbital velocity increases with increasing the

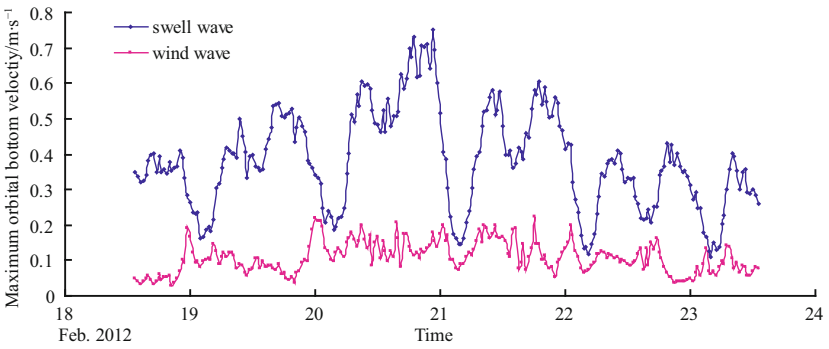

Fig.7. Maximum orbital bottom velocity of the swell and wind wave.

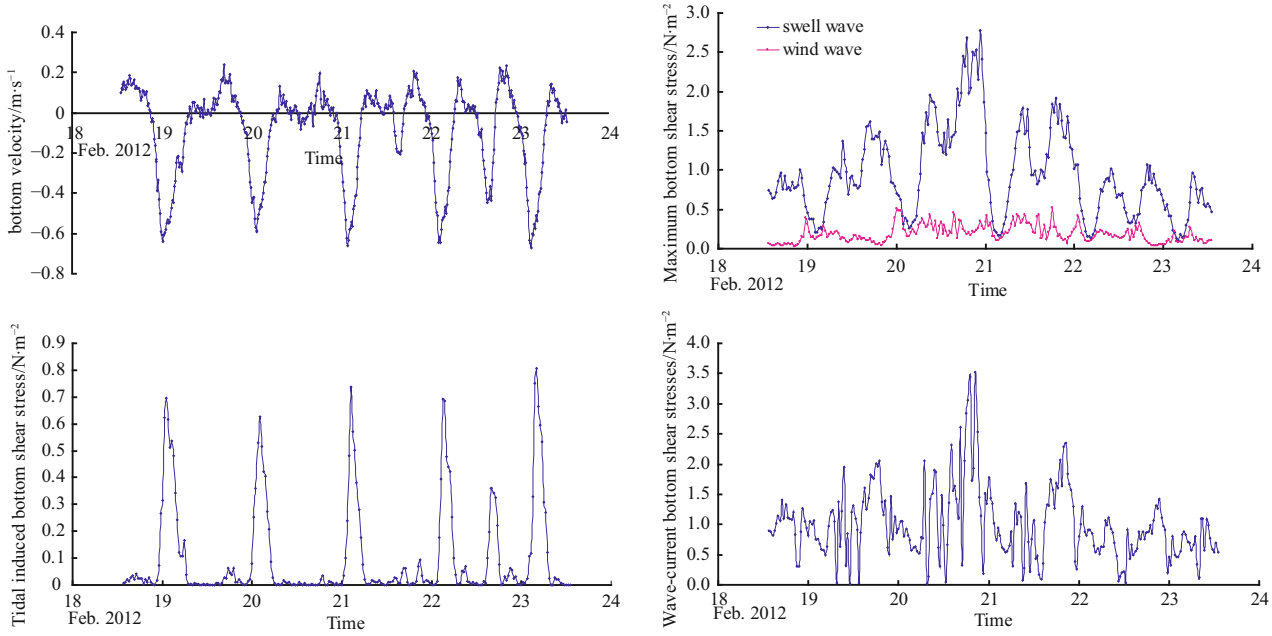

Fig.8. BSS at Sta. M3.

wave amplitude and the wave period. Since the wave-induced maximum BSS are proportional to the square of the maximum bottom orbital velocity, the swell with long periods is more important to the sediment re-suspension than the wind. So, the correlation between the SSC and the swell-induced shear stresses is stronger than that between the SSC and the wind-induced shear stresses.

Table 2. Correlation coefficient between BSS and SSC

Shear stress	Correlation coefficient
Wave-current	0.86
Swell	0.84
Wind	0.71
Tide	0.40

The peaks of the SSC appeared during 16:50–23:30 on February 20, exceeding 0.23 kg/m^3 on average, in correspondce with the peaks of the swell with the wave height being over 1 m. However, it was the neap tide during this period, and the tidal velocities were weak, only 0.2–0.4 m/s; the tidal-induced stresses were generally less than 0.1 N/m^2. Therefore, the high SSC was mainly caused by the swell-induced shear stresses.

6.2.3 *Effect of tidal current on SSC*

The tide at Sta. M3 is basically a progressive wave: the peak flood and the peak ebb appear 2 h ahead of the higher high tidal level and lower low tidal level respectively. The peaks of the SSC appeared around the high tidal level, and the low SSC appeared around the low tidal level, in right corresponce with the peaks of the tide-induced BSS, demonstrating that the effect of the tidal current on SSC is insignificant on the SSC (Fig. 9). The maximum SSC occurred at the highest wave height during the neap tide in the early days of the observation. In the later days of the observation, the spring tide was coming and the ebb velocity reached the maximum at 04:00 on February 23, but the SSC near the bottom was still low and less than 0.10 kg/m^3 due to the decrease of the wave height, further demonstrating that the effect of the tidal current on the SSC is insignificant.

The wave has been broken when it arrives at Sta. M3, at the inner slope of the mouth bar, so the wave height is consistent with the tide. When the tide is ebbing, the wave height is reduced due to the fall of the water depth: therefore, the wave shear stress is decreased; the direction of the tide is opposing the wave, which weakens the wave-current shear stresses. The opposite occurs when the tide is flooding. Generally, the flood

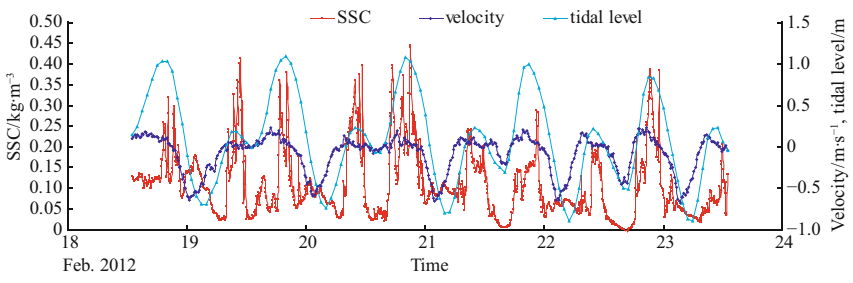

Fig.9. Bottom SSC, velocity and tidal level at Sta. M3.

tide enhances the wave shear stresses and increases the SSC near the bottom.

7 BSS effect on sediment re-suspension

During the measurement period, the surface sediment samples were obtained in the mouth bar area; four samples near Sta. M3 are selected to calculate the critical shear stresses in different grain sizes based on the formula by Cao et al. (2003).

Samples 28, 29 and 31 are mainly composed of the silt, representing the fine sediment, and Sample 30 is mainly composed of the sand, representing the coarse sediment in the mouth bar. As shown in Table 3, the critical shear stress for the fine sediment re-suspension is about 0.20 N/m^2, while that for the coarse sediment is about 0.30 N/m^2. The tidal currents are too weak to stir up the bottom sediment into the flow in most time except in the peak ebb and the peak flood, while the WCI is strong enough to re-suspend the coarse sediment (Fig. 10).

8 Discussion

The main findings in the BSS under the WCI in the ME are in agreement with those in the other coastal environments, such as the Cleveland Bay, North Australia (Lou and Ridd, 1996); the southern North Sea (Rosales et al., 2008); the Huanghe River Delta (Liang and Li, 2008). In the present study, the tidal contributions to the nonlinear WCI are higher than those in the Cleveland Bay. The tidal current contributions to the total BSS in ME are more than 11% and less than 10% in the Cleveland Bay, which shows that the tidal motion is more important in the ME environments.

Based on the field observations herein, the wave height fluctuates with the tidal level at the measurement site, which is in agreement with the model results by Wang et al. (2006) and similar to the Altamaha River (KiRyong and Daniela, 2006). According to Wang et al. (2006), the downstream of the estuary in the ZRD, the wave heights increase during the ebbing current and decrease during the flooding current. At the station near the river outlets, the high and low wave heights appear before the high tidal slack and low tidal slack respectively, by about 2–3 h. In the Altamaha River, after interacting with the shoaling region, the wave energy within the estuary becomes periodic in time with the greater wave energy during the flood to the high water phase of the tide and very low wave energy during the ebb to the low water (KiRyong and Daniela, 2006).

When waves break at a certain depth, there is a wave energy transformation. According to KiRyong and Daniela (2006), in the shallow water domain, the wave energy transformations are periodic with the tidal flow as waves propagate from the mid-shelf to the estuarine environment and interact with the current and the sea level height, which is consistent with our findings in the ME. From the outer slope to the top and inner slope of the mouth bar, crossing the shoaling region of the mouth bar, the wave energy transformations are periodic with the tidal flow, so the flood enhances the wave shear stresses.

The hydrodynamics in the ME during the dry season are wave and tide dominant while the runoff is weak. This study shows that the wave could dominate even at the inner slope of the mouth bar and become a main factor for the sediment transport, and the flood tide could help strengthen the BSS under the WCI. As a typical case in the ME, our study may provide a good reference for the similar estuaries in the world.

9 Conclusions

(1) The swell-induced BSS have been found to be the most important part of the BSS, accounting for 73% of the total BSS. The wind-induced BSS comes next, accounting for 16% of the total, and the tidal induced stress accounts for only 11% of the total.

(2) The correlation coefficient between the wave-current stress and the SSC is 0.86, and that between the current stresses and the SSC is only 0.40. The peaks of the SSC are strongly correlated to the height and BSS of the swell. The swell is the main

Table 3. Critical shear stresses for the sediment near the Sta. M3

Samples	median particle diameter/μm	critical shear stresses/N·m^{-2}
28	10.98	0.21
29	18.77	0.20
30	370.3	0.30
31	35.79	0.19

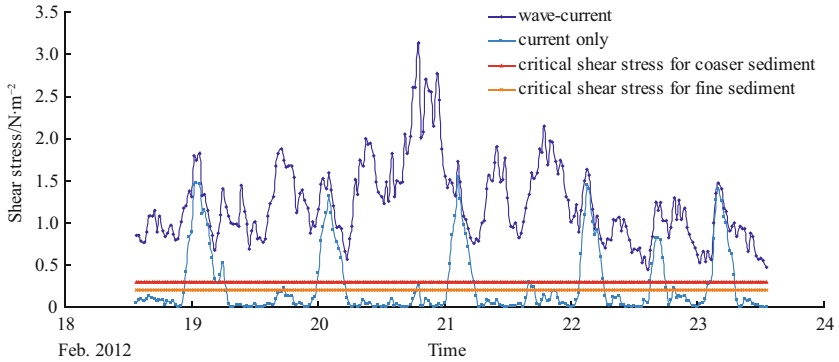

Fig.10. Critical shear stresses and BSS.

mechanism for the sediment re-suspension, and the tidal current effect on the sediment re-suspension is small.

(3) The peaks of the SSC are centered on the high tidal level, and the flood tide enhances the wave shear stresses and the SSC near the bottom.

(4) The critical shear stress for the fine sediment re-suspension is about 0.20 N/m^2, while that for the coarse sediment is about 0.30 N/m^2. Tidal currents are too weak to stir up the bottom sediment into the flow in most cases, but the WCI is strong enough to re-suspend the coarse sediment.

References

Cao Zude, Kong Lingshuang, Jiao Guiying. 2003. Initiation of sediment movement for a wave-current coexistent system. Acta Oceanologica Sinica (in Chinese), 25(3): 113–119

Christoffersen J B, Jonsson I G. 1985. Bed friction and dissipation in a combined current and wave motion. Ocean Engineering, 12(5): 387–423

Grant W D, Madsen O S. 1979. Combined wave and current interaction with a rough bottom. Journal of Geophysical Research, 84(C4): 1797–1808

Grant W D, Madsen O S. 1982. Movable bed roughness in unsteady oscillatory flow. Journal of Geophysical Research, 87(C1): 469–481

Hamblin P F. 1989. Observations and model of sediment transport near the turbidity maximum of the upper Saint Lawrence Estuary. Journal of Geophysical Research, 94: 14419–14428

Holmedal L E, Myrhaug D, Rue H. 2003. The sea bed boundary layer under random waves plus current. Continental Shelf Research, 23(7): 717–750

Jia Liangwen, Ren Jie, Xu Zhizhong, et al. 2009. Morphological evolution in recent years and waterway regulation of the sandbar area in the Modaomen Estuary. The Ocean Engineering (in Chinese), 27(3): 76–84

Jago C F, Jones S E, Rowden A A. 1992. Observations of suspended particulate dynamics in the southern North Sea. In: International Biennial Conference on Physics of Estuaries and Coastal Seas. Margaret River, Australia, extended abstract

Jonsson L G. 1966. Wave boundary layer and friction factors. In: 10th Proceeding Conference on Coastal Engineering Tokyo. New York: American Society of Civil Engineers, 127–148

KiRyong Kang, Daniela Di Iorio. 2006. Depth- and current-induced effects on wave propagation into the Altamaha River Estuary, Georgia. Estuarine, Coastal and Shelf Science, 66: 395–408

Kong Lingshuang, Cao Zude, Jiao Guiying, et al. 2003.The bottom shear stress and sediment movement for a wave-current coexisting system. Journal of Hydrodynamics (in Chinese), 18(1): 93–97

Liang Bingchen, Li Huajun. 2008. Bottom shear stress under wave-current interaction. Journal of Hydrodynamics, 20(1): 88–95

Li Chunchu. 1983. Dynamic and sedimentation of the Modaomen Estuary. Tropical Geography (in Chinese), 1: 27–34

Li Chunchu, Tian Xianping, Luo Xianlin, et al. 1993. Formation and evolution of the mouth bar and the regulation in the Modaomen estuary of the Xijiang river. In: Collection of the 7th National Symposium on Coastal Engineering (in Chinese). Beijing: China Ocean Press, 172–181

Lou Jing, Ridd Peter V. 1996. Wave-current bottom shear stresses and sediment resuspension in Cleveland Bay, Australia. Coastal Engineering, 29: 169–186.

Luo Xianlin, Li Chunchu, Tian Xianping. 1983. Wave characteristics and its impact on subaqueous delta of the Modaomen estuary of the Xijiang River. Journal of Sediment Research (in Chinese), 3: 53–60

Malarkey J, Davies A G. 1998. Modelling wave–current interactions in rough turbulent bottom boundary layers. Ocean Engineering, 25(2–3): 119–141

Mathisen P P, Madsen O S. 1996a. Waves and currents over a fixed ripple bed: 1. Bottom roughness experienced by waves in the presence and absence of currents. Journal of Geophysical Research, 101: 16533–16542

Mathisen P P, Madsen O S. 1996b.Waves and currents over a fixed ripple bed: 2. Bottom and apparent roughness experienced by currents in the presence of waves. Journal of Geophysical Research, 101: 16543–16550

Rosales P, Ocampo Torres F J, Osuna P, et al. 2008. Wave-current interaction in coastal waters: effects on the bottom-shear stress. Journal of Marine Systems, 71: 131–148

Rodolfo Bolaños, Peter D Thorne, Judith Wolf. 2012. Comparison of measurements and models of bed stress, bedforms and suspended sediments under combined currents and waves. Coastal Engineering, 62: 19–30

Shi John Z, Wang Yun. 2008. The vertical structure of combined wave–current flow. Ocean Engineering, 35: 174–181

Signell RP, Beardsley R C, Graber H C, et al. 1990. Effect of wave-current interaction on wind-driven circulation in narrow, shallow embayments. Journal of Geophysical Research, 95(C6): 9671–9678

Soulsby R L, Hamm L, Klopman G, et al. 1993. Wave-current interaction within and outside the bottom boundary layer. Coastal Engineering, 21: 41–69

Soulsby R. 1997. Dynamics of Marine Sands, a Manual for Practical Applications. London: Thomas Telford Publications

Styles R, Glenn S M. 2002. Modeling bottom roughness in the presence of wave-generated ripples. Journal of Geophysical Research, 107: 1950–1970

Swart D H. 1974. Offshore Sediment Transport and Equilibrium Beach Profiles. Delft Hydraulics Laboratory Publication, Delft, the Netherlands, 131

Trowbridge J, Madsen O S. 1984a. Turbulent wave boundary layer. 1. Model formulation and first-order solution. Journal of Geophysical Research, 89: 7989–7997

Trowbridge J, Madsen O S. 1984b. Turbulent wave boundary layer: 2. Second-order theory and mass transport. Journal of Geophysical Research, 89: 7999–8007

Wang Chonghao, Wai Winghong, Li Yoksheung, et al. 2006. Modeling of the wave-current interaction in the Pearl River estuary. Conference of Global Chinese Scholars on Hydrodynamics, Shanghai, China, 159–165